Corrosion Science 108 (2016) 194–199

Contents lists available at ScienceDirect

Corrosion Science

journal homepage: www.elsevier.com/locate/corsci

Dealloying monolithic Pt-Cu alloy to wire-like nanoporous structure for electrocatalysis and electrochemical sensing

Jiao-Jiao Gao [a], Gui-Ping Zhou [b], H.-J. Qiu [a,*], Y. Wang [a,*], J.Q. Wang [c,*]

[a] School of Chemistry and Chemical Engineering, Chongqing University, Chongqing 400044, China
[b] Grid construction training department, State Grid Technology college, Jinan 250003, China
[c] Ningbo Institute of Material Technology and Engineering, Chinese Academy of Sciences, Ningbo 315201, China

ARTICLE INFO

Article history:
Received 30 January 2016
Received in revised form 11 March 2016
Accepted 13 March 2016
Available online 16 March 2016

Keywords:
A: Alloy
B: TEM
C: De-alloying
Reduction

ABSTRACT

Micrometer wire-like PtCu catalysts with nanoporous structure and tunable composition were fabricated by dealloying Pt_3Cu_{97}. When the Pt:Cu ratio is lower than 1:99, dealloying results in dispersed PtCu nanoporous nanoparticles and/or single nanoparticles. Material characterization by X-ray diffraction and electron microscope shows that the formation of wire-like morphology is due to the large-scale shrink of the long rod-like alloy grains during the dealloying. The composition of the dealloyed nanoporous PtCu can be widely tuned by changing the concentration of the dealloying solution. Electrochemical test shows that the wire-like porous PtCu alloys show enhanced and composition-dependent catalytic activity for H_2O_2 electro-reduction.

1. Introduction

Pt-based nanomaterials have been attracting much research interest due to their important applications in fuel cells and electrochemical sensing/biosensing [1–8]. However, the low earth reservation of Pt greatly limits its practical applications. It has been found that alloying Pt with low-cost transition metals can reduce the using amount of Pt and more importantly, the alloying effect can significantly enhance the overall catalytic activity [9–15]. It is suggested that the compressively strained Pt-rich shell are responsible for the activity enhancement [14].

To synthesize Pt-based alloy nanomaterials, various methods such as one-pot solvothermal reduction, electro-deposition, etc., have been developed [1]. However, the precise control over the alloy composition and structure uniformity for activity optimization is still quite challenging by these bottom-up reduction methods. In recent years, dealloying has shown obvious advantage in fabricating nanostructured alloy catalysts with nanoporous ligament-pore structure [16–20]. Different from these bottom-up wet chemical reduction methods, dealloying can more precisely control the alloy ratio by selective removal of one component from a ternary alloy [21,22] or controlled dealloying a binary alloy [23,24]. Compared with limited single-phase ternary alloy systems, more binary systems are available for the dealloying to uniform nanoporous catalysts [25]. However, the nanoporous metals/alloys obtained by dealloying binary precursors usually only contain a few atomic percentage of active metal [20]. In order to widely tune the nanoporous alloy composition, a diluted binary alloy with more active metal seems to be a better precursor. For example, by controlled dealloying a diluted Au_5Ag_{95} alloy, nanoporous $Au_{50}Ag_{50}$ has been obtained [26]. However, this strategy still needs further studies.

Nanostructured Pt-Cu alloy has shown enhanced performance for various catalytic reactions such as electrochemical methanol oxidation and oxygen reduction [27–40]. In this work, we try to fabricate uniform nanoporous PtCu alloys with widely tuned alloy ratio by dealloying a diluted Pt-Cu binary precursor. Moreover, we explore the ratio limit of the Pt-Cu precursor for the formation of continuous nanoporous PtCu structure, which, as far as we know, has not been reported yet. It was interesting to find that with the decreasing Pt content in the precursor, the morphology of the dealloyed nanomaterials changed from monolithic nanoporous structure to aligned nanoporous micro-wires/rods and to nanoporous nanoparticles or simple nanoparticles. The results show that Pt_3Cu_{97} precursor is more suitable for the dealloying to control the composition of final nanoporous alloy. Electrochemical test shows that the nanoporous PtCu exhibits enhanced and composition-dependent catalytic activities for H_2O_2 reduction, which can be used for sensitive H_2O_2 sensing.

* Corresponding authors.
E-mail addresses: hjqiu@cqu.edu.cn (H.-J. Qiu), wangy@cqu.edu.cn (Y. Wang), jqwang@nimte.ac.cn (J.Q. Wang).

http://dx.doi.org/10.1016/j.corsci.2016.03.012
0010-938X/

2. Experimental section

Pt_1Cu_{99}, Pt_3Cu_{97}, $Pt_{15}Cu_{85}$ alloy ribbons (thickness: ~25 μm) were prepared by a melt-spinning technique using pure metals (purity: ≧99%) and a rotating Cu wheel (tagent speed is 20 m s^{-1}). The alloy ribbons were chemically dealloyed in HNO_3 solutions with different concentrations (12.6 M, 8.0 M, 1.6 M) for 24 h. The samples were characterized by X-ray diffraction (XRD, Bruker D8 Advanced X-ray diffractometer with Cu (Kα) radiation (λ = 1.5406 Å)), JEM-2100 high-resolution transmission electron microscope (HRTEM), and JSM-6700 field-emission scanning electron microscope (SEM, working potential: 15 kV) equipped with energy-dispersive X-ray spectrometer (EDS).

Electrochemical measurements were carried out on an electrochemical workstation (CHI 660e) with a three-electrode system. The prepared nanoporous metals-modified glassy carbon electrode (GCE) (3 mm in diameter), pure Pt electrode and saturated calomel electrode (SCE) were used as the working electrode, counter electrode, and reference electrode, respectively. All potentials used in this work were referred to SCE. The catalyst inks were prepared by mixing PtCu catalysts (3.0 mg), activated carbon (4.0 mg), isopropanol (300 μL), and Nafion solution (100 μL, 0.5 wt.%) for 30 min under sonication. The working electrode was prepared by dropping the catalyst ink (4 μL) on a GCE and dried at room temperature. The electrochemical active surface area (EASA) of Pt was calculated by integrating the charge associated with hydrogen adsorption between −0.1 and 0.1 V vs SCE. The adsorption of a monolayer of hydrogen on a polycrystalline Pt surface is 210 (μC cm^{-2}) [23].

3. Results and discussion

The compositions of all the precursors were controlled by the feeding amount of pure Cu and Pt and further confirmed by EDS (Fig. 1). A representative XRD pattern of the Pt_3Cu_{97} precursor is shown in Fig. 2. The three obvious diffraction peaks can be ascribed to (111), (200), and (220) diffraction of a face centered cubic (fcc) structure, indicating the single phase nature of the alloy ribbon, which is also in accordance with the Pt-Cu binary phase diagram. The three precursors were then dealloyed in concentrated HNO_3 solution. It is found that the dealloying of Pt_3Cu_{97} and $Pt_{15}Cu_{85}$ results in free-standing nanoporous metals with black color, whereas the dealloying of Pt_1Cu_{99} results in a cloudy solution. SEM images show that the morphology of the dealloyed $Pt_{15}Cu_{85}$ does not change obviously from that of the precursor (Fig. 3a). The alloy grains are well connected to each other. Only some cracks appear after the dealloying. This result is in good agreement with a general understanding that dealloying single-phase binary alloy with a suitable composition (noble component: ~15–45 at.%) does not affect the grain size and crystal orientation [19]. For the dealloyed Pt_3Cu_{97}, it was interesting to observe that well-aligned microcale wire-like structure with diameters from ~1 to 3 μm formed (Fig. 3b). The sample is in one piece after dealloying and a slight sonication or physical press can break it into micro-wire powder (Fig. 3c). The length of these wires is over 20 μm, which is in good agreement with the thickness of the precursor alloy. Since the Pt_3Cu_{97} precursor has a much higher amount of Cu, the formation of these micro-wires structure is due to the removal of a large amount of Cu, resulting in a big contraction of the PtCu grains (Fig. 3b) [23]. It is assumed that the large-scale removal of Cu by dealloying would produce a large amount of lattice void and/or dislocations within each grain. Thus, the collapse of lattice dislocations would then result in the plastic deformation, i.e., greatly reduced grain diameter [41]. The plastic deformation (grain size reduction) should also facilitate the diffusion and enrichment of Pt to form an interconnected ligament-pore structure within each wire-structured grain

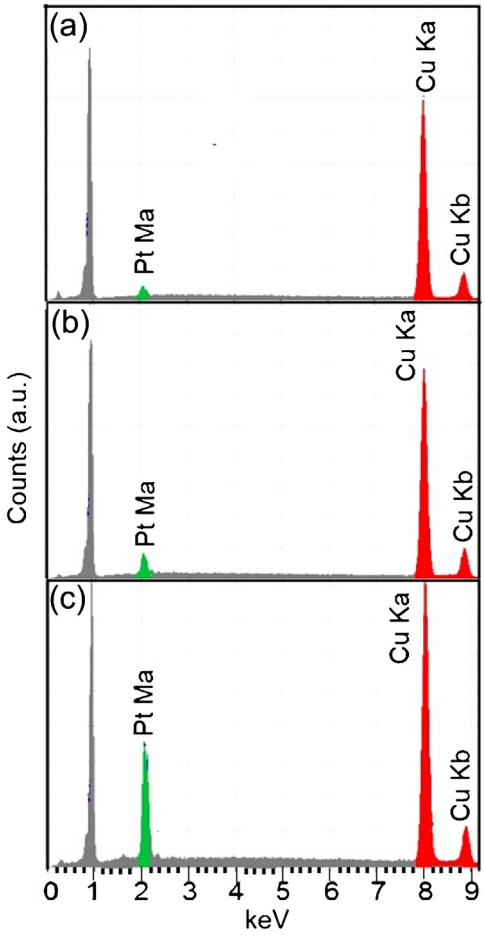

Fig. 1. EDS spectra of the PtCu precursors (Pt_1Cu_{99} (a); Pt_3Cu_{97} (b); $Pt_{15}Cu_{85}$ (c)).

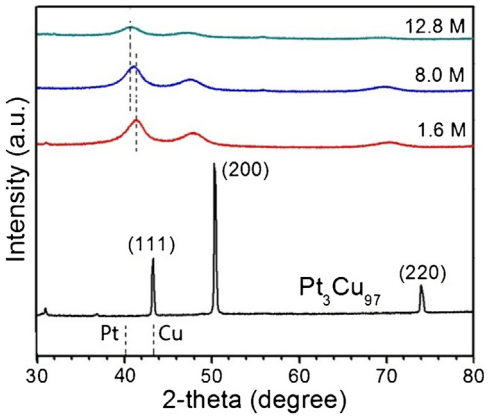

Fig. 2. XRD patterns of Pt_3Cu_{97} alloy before (a) and after (b) dealloying in HNO_3 solutions with different concentrations (1.6 M; 8.0 M; 12.8 M). The (111) diffractions of pure Pt and Cu are included for comparison.

instead of dispersed Pt nanoparticles. It is clear that when the Cu content increases from ~85 at.% to ~97 at.%, large-scale grain contraction has to occur during the formation of nanoporous structure by dealloying. Since the length of the formed wires is similar with the thickness of the alloy ribbon, the lateral contraction perpendicular to the <100> orientation seems more significant, resulting in separated individual wire-structured grains. When the Cu content increases to ~99 at.%, continuous nanoporous structure cannot be obtained at this dealloying condition. TEM analysis shows that the cloudy solution contains many nanoporous nanoparticles or simple

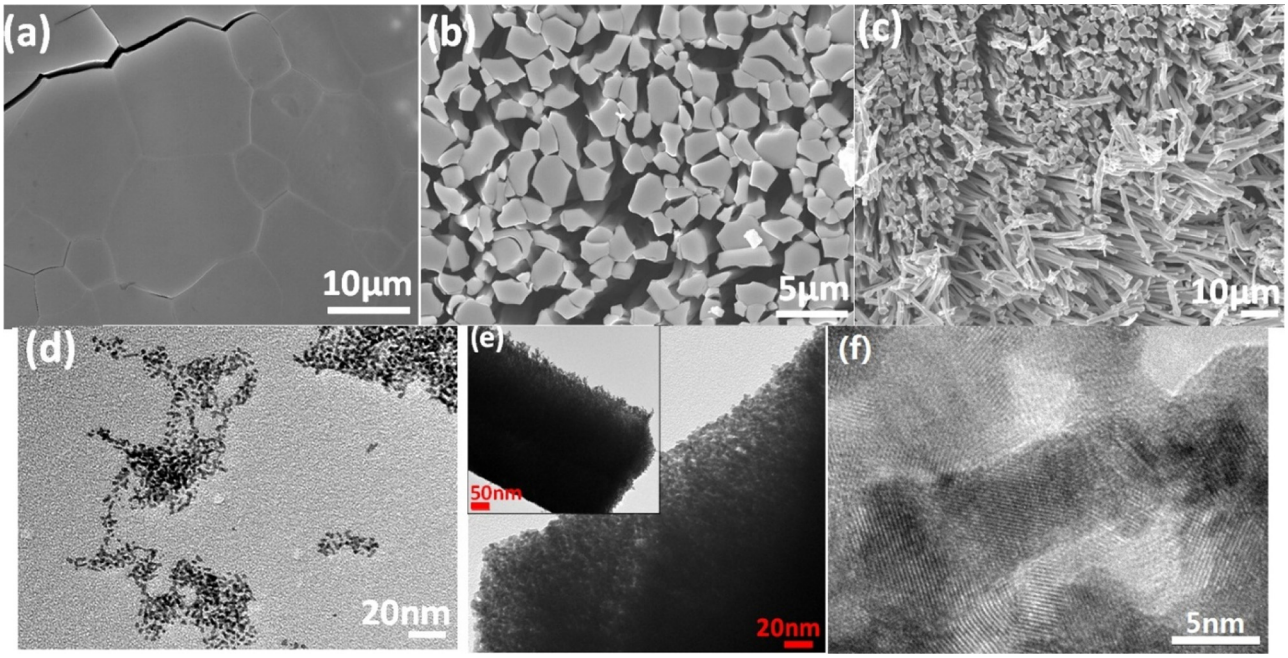

Fig 3. SEM images of the dealloyed $Pt_{15}Cu_{85}$ (a), and Pt_3Cu_{97} (b, c). TEM image of dealloyed Pt_1Cu_{99} (d), and Pt_3Cu_{97} (e). (f) HRTEM image of the nanoporous PtCu. Inset in (e) is the TEM image of single wire.

nanoparticles (Fig. 3d). This result indicates that when the content of Pt decreases to less than 1 at.%, the precursor is not suitable for the fast dealloying to continuous bulk nanoporous structure.

To analyze the microstructure of the formed PtCu wires, TEM characterization was carried out. Fig. 3e shows that uniform dark metallic ligaments and bright pores with a diameter of ~2 nm are across the entire wire, indicating the inherent nanoporous structure of each wire. The TEM image of one single micro-wire is shown in inset of Fig. 3e. Bright-field HRTEM image in Fig. 3f further demonstrate the ligament-pore structure by the clear contrast between dark metallic ligaments and brighter voids. The lattice fringe in the alloy ligaments can also be clearly observed.

To explore the effects of dealloying condition on the morphology/structure of the nanoporous wires, the Pt_3Cu_{97} was then etched by both chemical dealloying at different HNO_3 concentrations and electrochemical dealloying at different potentials in 0.5 M H_2SO_4 solution. It was found that chemical dealloying with different HNO_3 concentrations (12.6 M, 8 M, 1.6 M) had little effects on the morphology of the formed nanoporous microwires. Electrochemical linear sweep voltammetry curves in Fig. 4a show that pure Pt is very stable during the tested potential range. Alloying 3 at.% Pt in Cu slightly inhibit the electrochemical dissolution of Cu, exhibiting a higher onset potential and smaller current density compared with pure Cu. The Pt_3Cu_{97} can be steadily dealloyed when the applied potential over 0.15 V vs SCE. Thus, 0.2 and 0.4 V vs SCE were chosen for the electrochemical dealloying. It is observed that dealloying at a relatively low potential of 0.2 V vs SCE (i.e., low etching rate) also has negligible effect on the final morphology of the wires (Fig. 4b). These wires are well aligned with cylinder structure and the surface of each wire is smooth. However, when the dealloying potential increased to 0.4 V vs SCE, the cylinder-shaped grains became very thin and curved slightly and many micrometer-scale cracks appeared (Fig. 4c). It is known that under electrochemical fast dealloying condition, the dissolution of Cu becomes much faster, while the diffusion of Pt become even slower. Thus, the increased stress would cause these cracks [25]. The high potential and fast dissolution rate also cause a severe contraction of the alloy grain, leading to grain morphology change from cylinder to thin belt structure (Fig. 4c).

To study the dealloying condition on the composition of the wire-like nanoporous PtCu sample, the Pt_3Cu_{97} precursor was then free-dealloyed by different HNO_3 concentrations. By EDS analysis, it is found that the composition of the nanoporous PtCu wires depends on the concentration of the dealloying solution. The compositions are $Pt_{53}Cu_{47}$, $Pt_{60}Cu_{40}$, and $Pt_{70}Cu_{30}$, respectively, after dealloyed with 1.6 M, 8 M, and 12.8 M HNO_3. XRD analysis clearly shows that the diffraction peaks of all the three dealloyed samples shift to lower degree compared with those of the precursor due to the removal of large amount of Cu with a smaller atomic size (Fig. 2). These peaks locate between the diffraction peaks of pure Pt and pure Cu, indicating the alloy nature of the resulting material. The sample with a higher Cu content (dealloyed with a lower HNO_3 concentration) exhibits diffraction peaks at relatively higher degree. The peak positions are in good agreement with the value calculated by Vegard's law. All the diffraction peaks are broad suggesting the formation of nanostructure alloy ligaments.

The wire-like nanoporous Pt-Cu with different Pt/Cu ratios were then evaluated as electrocatalysts for the electro-reduction of H_2O_2 which is an essential mediator in food, pharmaceutical, clinical and various enzymatic reactions. Before the electrochemical reduction of H_2O_2, the catalysts were analyzed in 0.5 M H_2SO_4 solution. Fig. 5a shows cyclic voltammetry (CV) curves of three wire-like PtCu catalysts in 0.5 M H_2SO_4 solution. All the PtCu samples show characteristic CV curves of Pt. The peaks in the region between −0.1 and 0.1 V vs SCE can be ascribed to the adsorption and desorption of hydrogen. Between 0.1 and 0.3 V vs SCE is the double-layer region. When the potentials are higher than 0.3 V vs SCE, surface oxidation and subsequent reduction during the backward scan occur. For the PtCu catalyst with a higher Cu content, it is noticed that there is an obvious anodic peak at ~0.5 V during the forward scan, which is ascribed to the oxidation of residual surface Cu [42]. This peak does not change obviously during the first several CV scans in the acidic solution, suggesting that this small part of surface Cu is stabilized by neighboring Pt. Fig. 5b shows the CV curves of these catalysts in a PBS containing 40 mM H_2O_2. The current densities have been

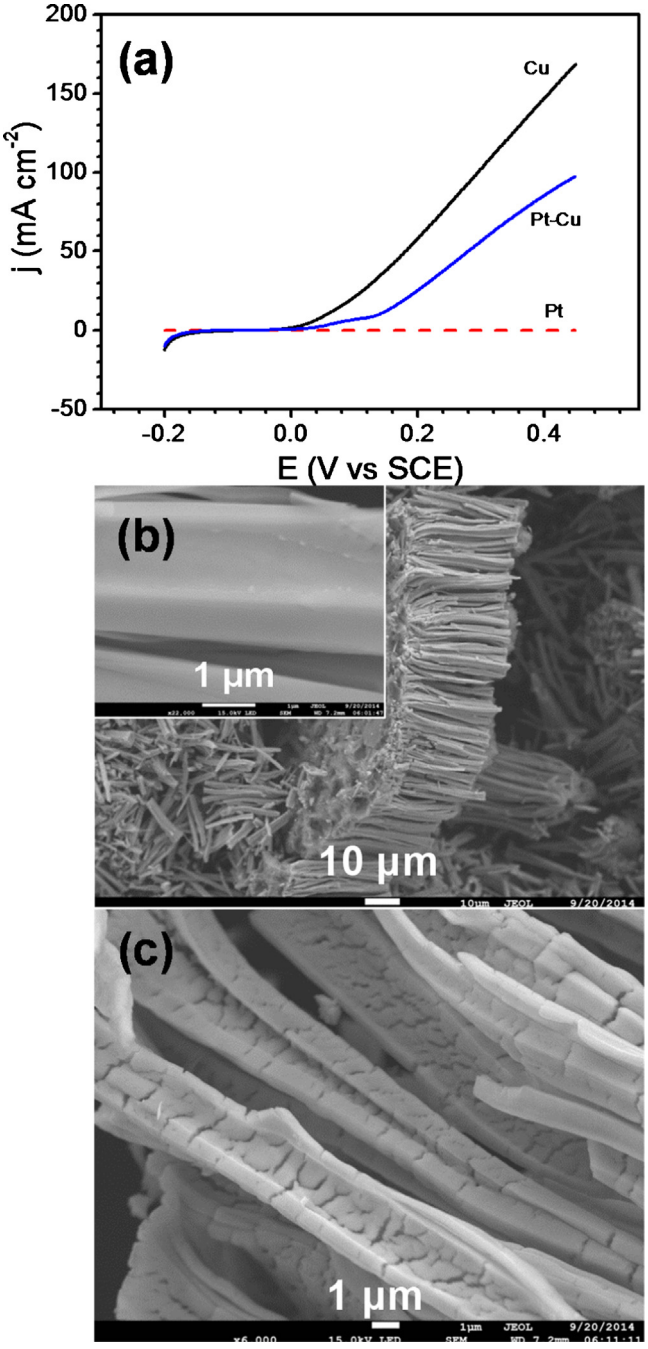

Fig. 4. Linear sweep voltammetry curve of Pt_3Cu_{97}, Pt, and Cu (a), and SEM images of the electrochemically dealloyed Pt_3Cu_{97} at 0.2 V (b) and 0.4 V (c) for 0.5 h. Inset in (b) shows the enlarged image of one wire surface.

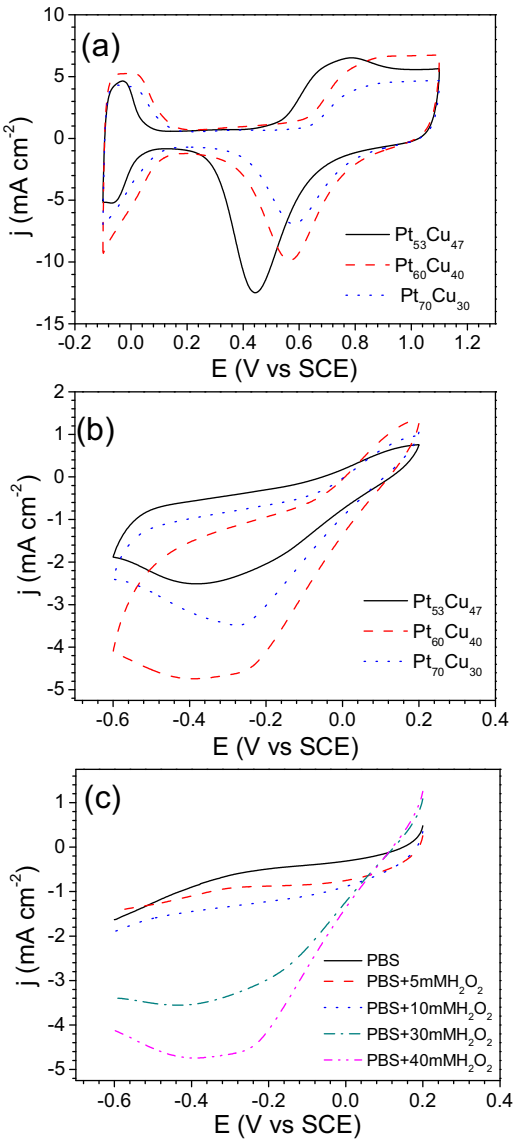

Fig. 5. CV curves of nanoporous $Pt_{53}Cu_{47}$, $Pt_{60}Cu_{40}$, and $Pt_{70}Cu_{30}$ in 0.5 M H_2SO_4 (a), 1 M PBS + 40 mM H_2O_2 solution (b) and linear sweep voltammetry curves of $Pt_{60}Cu_{40}$ in 1 M PBS with different H_2O_2 concentrations (c). Scan rate: 50 mV s^{-1}.

normalized by the EASA of Pt. After the addition of H_2O_2, there is a clear reduction peak between ~−0.4 and −0.1 V vs SCE for all the three samples, suggesting the high catalytic activities. In comparison, the $Pt_{60}Cu_{40}$ sample shows the highest current density and positively shifted peak potentials, indicating the best catalytic activity of this sample. Fig. 5c records the current change of the catalyst with the increasing H_2O_2 concentrations. It was observed that the current for H_2O_2 reduction increased sensitively with the increase of the H_2O_2 concentration, suggesting the potential of the electrode for H_2O_2 sensing. Fig. 6a shows the amperometric responses of the $Pt_{60}Cu_{40}$ electrode on successive addition of H_2O_2 in a stirring PBS at −0.2 V vs SCE. The current of electrode responses rapidly with each addition of 0.5 mM H_2O_2 and reaches the steady-state current within 5 s. As shown in Fig. 6b, the wire-like nanoporous $Pt_{60}Cu_{40}$ electrode exhibits a linear response to H_2O_2 concentration up to ~7.0 mM (R = 0.995) with a detection limit of ~2 μM. The linear range is wider than some graphene and carbon nanotube-based H_2O_2 sensors [43].

The high catalytic performance of the wire-like nanoporous PtCu should result from the following aspects. Firstly, the continuous PtCu network and pore channels in each wire make all the active Pt surface sites available for the catalytic reaction and also facilitates the mass and electron transfer. Secondly, an optimized PtCu alloy ratio can greatly enhance the catalytic reactivity as a result of possible electronic, strain, or alloy effects [44]. It is known that alloying Pt with other metals can lower the electronic binding energy in Pt and promote the catalytic activity. Thirdly, one-dimensional structure (such as nanowires and nanorods) has been reported to possess enhanced catalytic activity due to their uniquely anisotropic nature [45].

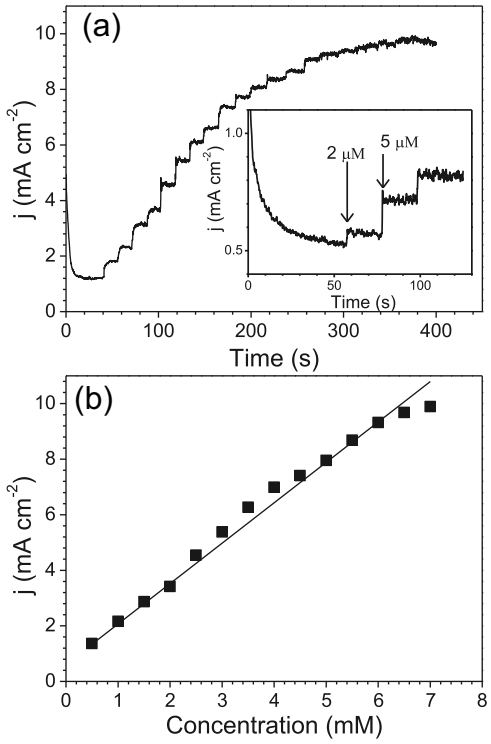

Fig. 6. I-t curves of the $Pt_{60}Cu_{40}$ electrode with the continuous addition of 0.5 mM H_2O_2 (a) and the corresponding calibration curve. Inset in (a) the current response to 2 μM and 5 μM H_2O_2.

4. Conclusions

By dealloying binary PtCu precursors with different alloy ratios, nanoporous metals with different morphologies were obtained. Dispersed nanoporous nanoparticles or single nanoparticles were obtained from Pt_1Cu_{99} precursor. Aligned wire-like PtCu with continuous nanoporous structure was fabricated from a Pt_3Cu_{97} precursor, which was due to the large contraction of the PtCu alloy grains. The composition of the nanoporous wires can be tuned by changing the concentration of dealloying solutions. Importantly, when tested as a potential cathode catalyst for H_2O_2 reduction, the wire-like nanoporous PtCu catalysts showed enhanced and composition-dependent activity with $Pt_{60}Cu_{40}$ exhibiting the best performance. The present strategy (without the use of any organic solvent or surfactant) may provide a simple way to synthesize nanocatalysts.

Acknowledgement

We thank the financial support from Chongqing basic and frontier research project (cstc2015jcyjA50026), Thousand Young Talents Program of the Chinese Central Government (No. 0220002102003), and National Natural Science Foundation of China (NSFC, No. 21373280).

References

[1] A. Chen, P. Holt-Hindle, Platinum-based nanostructured materials: synthesis, properties, and applications, Chem. Rev. 110 (2010) 3767–3804.
[2] J. Snyder, T. Fujita, M.W. Chen, J. Erlebacher, Oxygen reduction in nanoporous metal-ionic liquid composite electrocatalysts, Nat. Mater. 9 (2010) 904–907.
[3] Y. Lu, Y. Jiang, H. Wu, W. Chen, Nano-PtPd cubes on graphene exhibit enhanced activity and durability in methanol electrooxidation after CO stripping–cleaning, J. Phys. Chem. C 117 (2013) 2926–2938.
[4] S.E. Bozbag, U. Unal, M.A. Kurykin, C.J. Ayala, M. Aindow, C. Erkey, Thermodynamic control of metal loading and composition of carbon aerogel supported Pt–Cu alloy nanoparticles by supercritical deposition, J. Phys. Chem. C 117 (2013) 6777–6787.
[5] Y. Kuang, Z. Cai, Y. Zhang, D. He, X. Yan, Y. Bi, Y. Li, Z. Li, X. Sun, Ultrathin dendritic Pt_3Cu triangular pyramid caps with enhanced electrocatalytic activity, ACS Appl. Mater. Interfaces 6 (2014) 17748–17752.
[6] Y. Shiraishi, H. Sakamoto, Y. Sugano, S. Ichikawa, T. Hirai, Pt–Cu bimetallic alloy nanoparticles supported on anatase TiO_2: highly active catalysts for aerobic oxidation driven by visible light, ACS Nano 7 (2013) 9287–9297.
[7] J. Wu, H. Yang, Platinum-based oxygen reduction electrocatalysts, Acc. Chem. Res. 46 (2013) 1848–1857.
[8] Z. Zhu, Y. Zhai, S. Dong, Facial synthesis of PtM (M = Fe, Co, Cu, Ni) bimetallic alloy nanosponges and their enhanced catalysis for oxygen reduction reaction, ACS Appl. Mater. Interfaces 6 (2014) 16721–16726.
[9] M. Gong, G. Fu, Y. Chen, Y. Tang, T. Lu, Autocatalysis and selective oxidative etching induced synthesis of platinum–copper bimetallic alloy nanodendrites electrocatalysts, ACS Appl. Mater. Interfaces 6 (2014) 7301–7308.
[10] S. Guo, S. Sun, FePt nanoparticles assembled on graphene as enhanced catalyst for oxygen reduction reaction, J. Am. Chem. Soc. 134 (2012) 2492–2495.
[11] Y. Kang, J.B. Pyo, X. Ye, T.R. Gordon, C.B. Murray, Synthesis, shape control, and methanol electro-oxidation properties of Pt–Zn alloy and Pt_3Zn intermetallic nanocrystals, ACS Nano 6 (2012) 5642–5647.
[12] B.Y. Xia, H.B. Wu, X. Wang, X.W. Lou, One-pot synthesis of cubic $PtCu_3$ nanocages with enhanced electrocatalytic activity for the methanol oxidation reaction, J. Am. Chem. Soc. 134 (2012) 13934–13937.
[13] S. Koh, P. Strasser, Electrocatalysis on bimetallic surfaces: modifying catalytic reactivity for oxygen reduction by voltammetric surface dealloying, J. Am. Chem. Soc. 129 (2007) 12624–12625.
[14] K.C. Neyerlin, R. Srivastava, C. Yu, P. Strasser, Electrochemical activity and stability of dealloyed Pt–Cu and Pt–Cu–Co electrocatalysts for the oxygen reduction reaction (ORR), J. Power Sources 186 (2009) 261–267.
[15] L. Su, S. Shrestha, Z.H. Zhang, W. Mustain, Y. Lei, Platinum-copper nanotube electrocatalyst with enhanced activity and durability for oxygen reduction reactions, J. Mater. Chem. A 1 (2013) 12293–12301.
[16] W. Liu, L. Chen, J. Yan, N. Li, S. Shi, S. Zhang, Dealloying solution dependence of fabrication, microstructure and porosity of hierarchical structured nanoporous copper ribbons, Corros. Sci. 94 (2015) 114–121.
[17] N.T. Tuan, J. Park, J. Lee, J. Gwak, D. Lee, Synthesis of nanoporous Cu films by dealloying of electrochemically deposited Cu–Zn alloy films, Corros. Sci. 80 (2014) 7–11.
[18] Z. Zhao, J. Xu, C. Shang, R. Ye, Y. Wang, Dealloying-dirven synthesis of sea-urchin like titanate nanowires and hierarchically porous anatase TiO_2 nanospindles with enhanced photocatalytic performance, Corros. Sci. 98 (2015) 651–660.
[19] H.-J. Qiu, J.Q. Wang, P. Liu, Y. Wang, M.W. Chen, Hierachical nanoporous metal/metal-oxide composite by dealloying metallic glass for high-performance energy storage, Corros. Sci. 96 (2015) 196–202.
[20] R. Li, X. Liu, H. Wang, Y. Wu, Z.P. Lu, Bendable nanoporous copper thin films with tunable thickness and pore features, Corros. Sci. 104 (2016) 227–235.
[21] X. Li, H.J. Qiu, J.Q. Wang, Y. Wang, Corrosion of ternary Mn–Cu–Au to nanoporous Au–Cu with widely tuned Au/Cu ratio for electrocatalyst, Corros. Sci. (2016), http://dx.doi.org/10.1016/j.corsci.2016.01.025.
[22] Z. Zhang, C. Zhang, J. Sun, T. Kou, Q. Bai, Y. Wang, Y. Ding, Ultrafine nanoporous PdFe/Fe_3O_4 catalysts with doubly enhanced activities towards electro-oxidation of methanol and ethanol in alkaline media, J. Mater. Chem. A 1 (2013) 3620–3628.
[23] H.J. Qiu, X. Shen, J.Q. Wang, A. Hirata, T. Fujita, Y. Wang, M.W. Chen, Aligned nanoporous Pt–Cu bimetallic microwires with high catalytic activity toward methanol electrooxidation, ACS Catal. 5 (2015) 3779–3785.
[24] X.B. Ge, L.Y. Chen, J.L. Kang, T. Fujita, A. Hirata, W. Zhang, J.H. Jiang, M.W. Chen, A core–shell nanoporous Pt–Cu catalyst with tunable composition and high catalytic activity, Adv. Funct. Mater. 23 (2013) 4156–4162.
[25] H.J. Qiu, L. Peng, X. Li, H.T. Xu, Y. Wang, Using corrosion to fabricate various nanoporous metal structures, Corros. Sci. 92 (2015) 16–31.
[26] Z. Qi, J. Weissmüller, Hierarchical nested-network nanostructure by dealloying, ACS Nano 7 (2013) 5948–5954.
[27] E.J. Coleman, M.H. Chowdhury, A.C. Co, Insights into the oxygen reduction reaction activity of Pt/C and PtCu/C catalysts, ACS Catal. 5 (2015) 1245–1253.
[28] I. Dutta, M.K. Carpenter, M.P. Balogh, J.M. Ziegelbauer, T.E. Moylan, M.H. Atwan, N.P. Irish, Electrochemical and structural study of a chemically dealloyed PtCu oxygen reduction catalyst, J. Phys. Chem. C 114 (2010) 16309–16320.
[29] J.A. Wittkopf, J. Zheng, Y. Yan, High-performance dealloyed PtCu/CuNW oxygen reduction reaction catalyst for proton exchange membrane fuel cells, ACS Catal. 4 (2014) 3145–3151.
[30] D. Chen, Y. Zhao, X. Peng, X. Wang, W. Hu, C. Jing, S. Tian, J. Tian, Star-like PtCu nanoparticles supported on graphene with superior activity for methanol electro-oxidation, Electrochim. Acta 177 (2015) 86–92.
[31] H. Liu, S. Wang, F. Jia, Conversion of commercial Pt/C to clean Pt–Cu/C catalyst with high activity toward methanol oxidation, Electrochim. Acta 184 (2015) 331–337.
[32] L. Liu, G. Samjeské, S. Takao, K. Nagasawa, Y. Iwasawa, Fabrication of PtCu and PtNiCu multi-nanorods with enhanced catalytic oxygen reduction activities, J. Power Sources 253 (2014) 1–8.
[33] A. Marcu, G. Toth, R. Srivastava, P. Strasser, Preparation, characterization and degradation mechanisms of PtCu alloy nanoparticles for automotive fuel cells, J. Power Sources 208 (2012) 288–295.

[34] Z.L. Zhao, L.Y. Zhang, S.J. Bao, C.M. Li, One-pot synthesis of small and uniform Au@PtCu core–alloy shell nanoparticles as an efficient electrocatalyst for direct methanol fuel cells, Appl. Catal. B 174–175 (2015) 361–366.
[35] K. Eid, H. Wang, P. He, K. Wang, T. Ahamad, S.M. Alshehri, Y. Yamauchi, L. Wang, One-step synthesis of porous bimetallic PtCu nanocrystals with high electrocatalytic activity for methanol oxidation reaction, Nanoscale 7 (2015) 16860–16866.
[36] W. Hong, C. Shang, J. Wang, E. Wang, Trimetallic PtCuCo hollow nanospheres with a dendritic shell for enhanced electrocatalytic activity toward ethylene glycol electrooxidation, Nanoscale 7 (2015) 9985–9989.
[37] H.J. Qiu, H.T. Xu, X. Li, J.Q. Wang, Y. Wang, Core–shell-structured nanoporous PtCu with high Cu content and enhanced catalytic performance, J. Mater. Chem. A 3 (2015) 7939–7944.
[38] S.-H. Ye, X.-J. He, L.-X. Ding, Z.-W. Pan, Y.-X. Tong, M. Wu, G.-R. Li, Cu_2O template synthesis of high-performance PtCu alloy yolk–shell cube catalysts for direct methanol fuel cells, Chem. Commun. 50 (2014) 12337–12340.
[39] X. Zhao, B. Luo, R. Long, C. Wang, Y. Xiong, Composition-dependent activity of Cu–Pt alloy nanocubes for electrocatalytic CO_2 reduction, J. Mater. Chem. A 3 (2015) 4134–4138.
[40] J. Sun, J. Shi, J. Xu, X. Chen, Z. Zhang, Z. Peng, Enhanced methanol electro-oxidation and oxygen reduction reaction performance of ultrafine nanoporous platinum–copper alloy: experiment and density functional theory calculation, J. Power Sources 279 (2015) 334–344.
[41] S. Parida, D. Kramer, C.A. Volkert, H. Rosner, J. Erlebacher, J. Weissmuller, Volume change during the formation of nanoporous gold by dealloying, Phys. Rev. Lett. 97 (2006) 035504.
[42] C. Xu, A. Liu, H.-J. Qiu, Y. Liu, Nanoporous PdCu alloy with enhanced electrocatalytic performance, Electrochem. Commun. 13 (2011) 766–769.
[43] X.C. Dong, Y.W. Ma, G.Y. Zhu, Y.X. Huang, J. Wang, M.B. Chan-Park, L.H. Wang, W. Huang, P. Chen, Synthesis of graphene-carbon nanotube hybrid foam and its use as a novel three-dimensional electrode for electrochemical sensing, J. Mater. Chem. 22 (2012) 17044–17048.
[44] H.J. Qiu, H.-T. Xu, L. Liu, Y. Wang, Correlation of the structure and applications of dealloyed nanoporous metals in catalysis and energy conversion/storage, Nanoscale 7 (2015) 386–400.
[45] C. Koenigsmann, E. Sutter, T.A. Chiesa, R.R. Adzic, S.S. Wong, Highly enhanced electrocatalytic oxygen reduction performance observed in bimetallic palladium-based nanowires prepared under ambient, surfactantless conditions, Nano Lett. 12 (2012) 2013–2020.